Chapter 5

Characteristic observations in Arsenic functionalized diatoms

5.1 Detection of arsenic using diatom frustules

In this Chapter, report is made of the investigations on the modification of chemical composition of a representative diatom *Cosmioneis reimeri* by arsenic compounds. The work was conducted to investigate the ability of diatom frustules to incorporate arsenic into the diatom frustules in their growth process. The culture and cleaning processes of diatoms were as described in section 2.2 and 2.3 of chapter 2 respectively. The effect of arsenic treatment in diatoms was studied by adding 1mM solution of Sodium Arsenite ($NaAsO_2$) to 250ml of the cultured medium. The optical properties of diatom frustules, when treated with arsenic compound, changed. This might find new application in optical nanobiotechnology. In this work however only the characteristic changes of arsenic treated diatom frustules as compared to the untreated diatom frustules were investigated.

5.2 Optical microscopy, SEM and EDX analyses of diatom frustules

The presence of pennate shaped diatoms was confirmed by optical microscopy analysis with a magnification of 100x. Figure 5.1 shows the optical microscopy images of the diatoms in a biological colony. Figure 5.2 shows the SEM micrographs of the valves of the frustule of a *Cosmioneis reimeri* diatom species cleaned by hydrogen peroxide and hydrochloric acid treatment. It was observed that there were two connected lanceolate valves with slightly rounded and protected end. Moreover, the frustules contained nanoscale size rounded areolae, a slightly wider central area with narrow axial area. With these observations and comparing with diatom identification guide and ecological resource database [1], the diatom species was confirmed to be fresh water *Cosmioneis reimeri.* The approximate length of the cells was around 15 μm to 20μm and thickness of the silica cell was about 2.5μm to 3μm. The diameter of pores was approximately 100nm to 400nm.

The SEM-EDS spot analysis, as obtained in figure 5.3, confirmed that diatom frustules were mainly composed of silicon in the form of silica (SiO_2). Moreover the presence of arsenic was confirmed by the characteristic L-energy peaks as shown in figure 5.3(b).

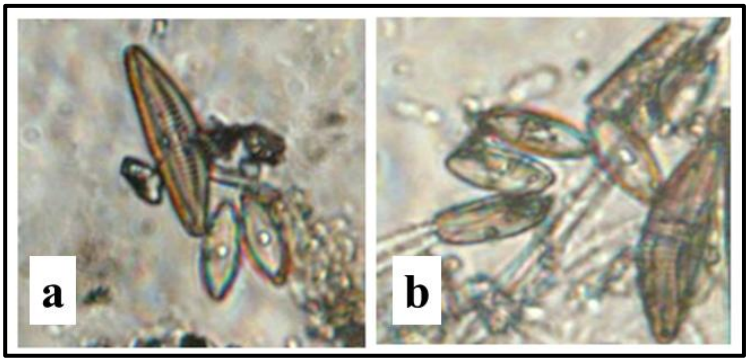

Figure 5.1 (a & b) Optical microscopy images of pennate diatoms in a biological colony with magnification 100x.

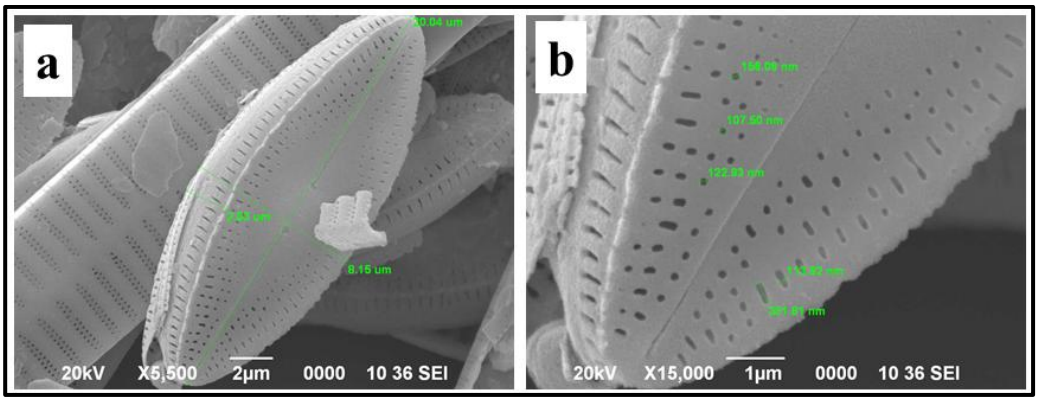

Figure 5.2 (a & b) SEM micrographs of *Cosmioneis reimeri* diatom frustules.

5.3 XRD analysis of arsenic treated and untreated diatom frustules

Presence of arsenic was also confirmed in arsenic treated diatom frustules by XRD analysis when untreated and arsenic treated diatom frustules were subjected to X-ray probe to elucidate the chemical nature of the modification in the range of diffraction angle (2θ) between 20º and 70º. Contrary to the amorphous untreated diatom frustules, the XRD spectrum (shown in figure 5.4) for arsenic treated diatom frustules showed distinct peaks at Bragg angle of 25.27º and 44.11º, which correspond to the presence of arsenic crystallites (1999 JCPDS no. 03-0754). The crystallite size (D) was calculated by using the Debye-Scherrer formula given in equation 3.1 and 3.2 in chapter 3. Bragg angle 25.27º was chosen to calculate the crystallite size of arsenic nanoparticles which was approximately 29 nm.

5.4 FTIR analysis of arsenic treated and untreated diatom frustules

The investigations on the chemical character in terms of bond information of the nanoporous untreated diatom frustules and sodium arsenite incorporated diatom frustules were carried out at ambient temperature by means of Fourier Transform Infrared (FTIR) Spectroscopy (shown in figure 5.5). Band assignments were performed by comparing the band positions with the values found in literature and listed in table 5.1. In consistence with the previous reports [2-3], the FTIR spectra reported here clearly showed the characteristic absorption peaks for diatom frustules. In addition to these peaks, characteristic peaks for arsenic was also observed in the FTIR spectrum for the arsenic treated diatom frustules, which was the main focus of the FTIR study.

The observed peaks at 463cm^{-1} and 1022cm^{-1} for untreated and peaks at 466cm^{-1}, 691cm^{-1}, 1029cm^{-1} and 1071cm^{-1} for the arsenic treated diatom frustules are assigned to the stretching vibrations of Si-O in Si-O-Si [5]. The peak at 530cm^{-1} is probably due to the out of plane Si-O-Si bending vibrations [5, 6]. This is attributed to the presence of siloxane functional group in the diatom frustules. The peaks at 769cm^{-1}, 1383cm^{-1} for untreated and at 748cm^{-1} and 1385cm^{-1} for the arsenic treated diatom frustules are assigned to the -CH_2 rocking [7]. The strong absorption peak at 1630cm^{-1} for both untreated and arsenic treated frustules represents the NH_2 bending for primary amide group of residual proteins associated with diatom biosilica[2,4,7]. This could include the “silaffin” class of silica precipitation proteins imbedded within diatom biosilica [2]. The 1630cm^{-1} peak could also be due to -CN stretching, N-H bending and/or carbonyl [-CO] stretching for secondary amides [7]. The peaks observed at 1383cm^{-1} and 2918cm^{-1} for untreated

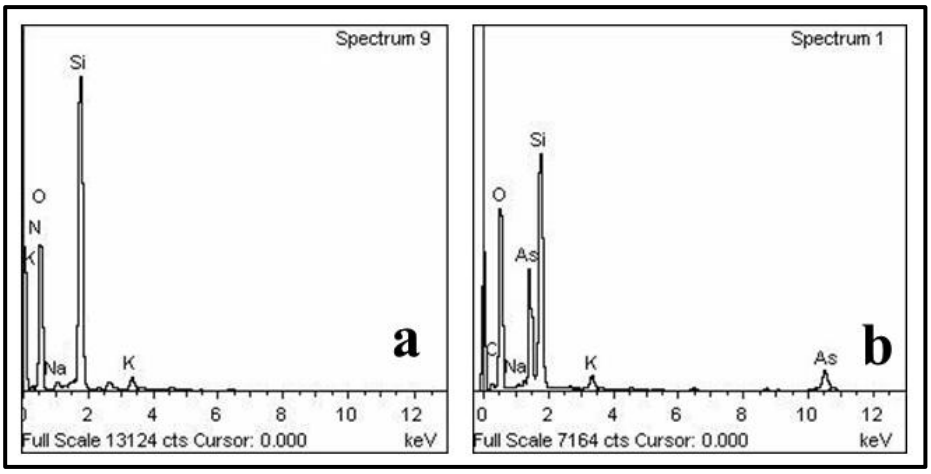

Figure 5.3 Energy dispersive X-ray spectroscopy of (a) untreated and (b) arsenic treated diatom frustule.

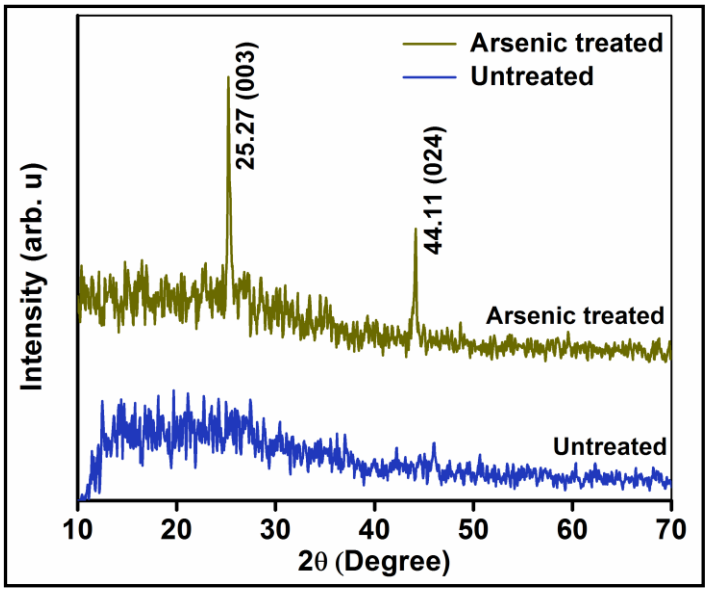

Figure 5.4 XRD diffractrogram of untreated and arsenic treated diatom frustules.

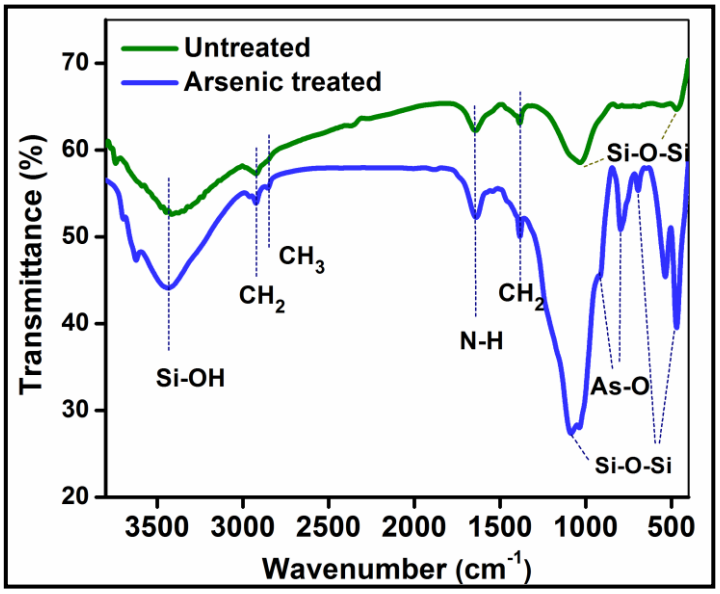

Figure 5.5 FTIR spectra of untreated and arsenic treated frustule biosilica in transmission mode.

Table 5.1 Results of functional group analysis by FTIR

Untreated diatoms Wave-number (cm^{-1})	Functional groups	Corresponding structure	Arsenic treated Frustules Wavenumber (cm^{-1})	Functional groups	Corresponding structure
463	Silica	Si-O-Si stretching	466,691	Silica	Si-O-Si stretching
-	-	-	530	Siloxane	Si-O-Si bending (out of plane)
-	-	-	796, shoulder at 909		As-O stretching vibration
1022	Silica	Si-O-Si stretching	1029, 1071	Silica	Si-O-Si stretching
1383	Aliphatic	CH_2 rocking	1385	Aliphatic	CH_2 rocking
1630	Amine	NH_2 bending (primary) and N-H bending (secondary), -CN stretching (secondary)	1630	Amine	NH_2 bending (primary) and N-H bending (secondary), -CN stretching (secondary)
2847	Aliphatic	CH_3 symmetric stretching	2849	Aliphatic	CH_3 symmetric stretching
2918	Aliphatic	CH_2 asymmetric stretching	2920	Aliphatic	CH_2 asymmetric stretching
3408, 3728	Silanol	Si-O-H stretching	3430, 3618, 3684	Silanol	Si-O-H stretching

and 1385cm^{-1}, 2849cm^{-1} and 2920cm^{-1} for arsenic treated diatom frustules are assigned to -CH_3 and/or -CH_2 symmetric and asymmetric stretching of aliphatic functional group [5, 7-9]. These asymmetric and symmetric stretching modes of -CH are mostly related to the carbon chain of organo-silane molecules in the diatom frustules. A general widening of the bands at around 3430cm^{-1} is observed which is also reported in similar studies of diatom frustule in previous works [5]. The peaks at 3728cm^{-1}, 3408cm^{-1} for untreated diatom frustules and 3430cm^{-1}, 3618cm^{-1}, 3684cm^{-1} for arsenic treated diatom frustules suggest the presence of silanol [Si-OH] groups in the diatom frustules. However, no characteristic peaks were found in the range 2100-2360cm^{-1}, which is for Si-H stretching of Silane group. The shifting of absorption peaks due to O-H stretching, vibration of Si-OH group and that of Si-O-Si group after insertion of arsenic indicate the involvement of Si-OH groups during the adsorption of arsenic. In addition to this, a distinct band at 780-796cm^{-1} and a shoulder at 909cm^{-1} in case of arsenic treated diatom frustules were observed which can be assigned to the stretching vibrations of the As-O bond [10].

5.5 UV-visible spectroscopic analysis of arsenic treated and untreated diatom frustules

It was observed from the UV-Vis spectra of untreated diatom frustules that intense absorption occurred near 242nm(UV region) and then intensity decreased with increasing wavelength which was due to the electronic transition from non-bonding orbitals to pi anti-bonding orbitals. These results indicated strong quantum confinement (QC) of the carrier in the porous silica layers, which is due to the smaller dimension of porous structure of silica as compared to bulk silica [11]. However, two absorption peaks were observed near 213nm and 256nm in case of arsenic treated sample. Peak at 213nm was due to electronic transition from pi bonding orbitals of As-As double bond to pi anti-bonding orbitals [12] and peak at 256nm was also due to electronic transition from non-bonding orbitals to pi anti-bonding orbitals. The non-bonding orbital has a higher energy than a pi bonding orbital. That means the transition from a lone pair to pi anti-bonding orbital needs less energy. The absorption is considered to be an interaction between the light and inner nanostructure [13]. It is noteworthy to mention that, broad transitions need more energy and, therefore, absorb light with shorter wavelengths. Molecules containing pi bonds or atoms with non-bonding orbitals can absorb the energy in the form of UV or visible light to excite these electrons to higher anti-bonding molecular orbitals. A non-bonding orbital is a lone pair. The more easily excited the electrons, the longer the wavelength of light it can absorb.

The possible electronic transitions are shown below (The schematic of hypothetical energy diagram of electronic transition is shown in figure 5.6.).

(1) $\pi \xrightarrow{\text{to}} \pi^*$ (pi bonding orbitals to pi anti-bonding orbitals)

(2) $n \xrightarrow{\text{to}} \pi^*$ (non-bonding orbitals to pi anti-bonding orbitals)

(3) $n \xrightarrow{\text{to}} \sigma^*$ (non-bonding orbitals to sigma anti-bonding orbitals)

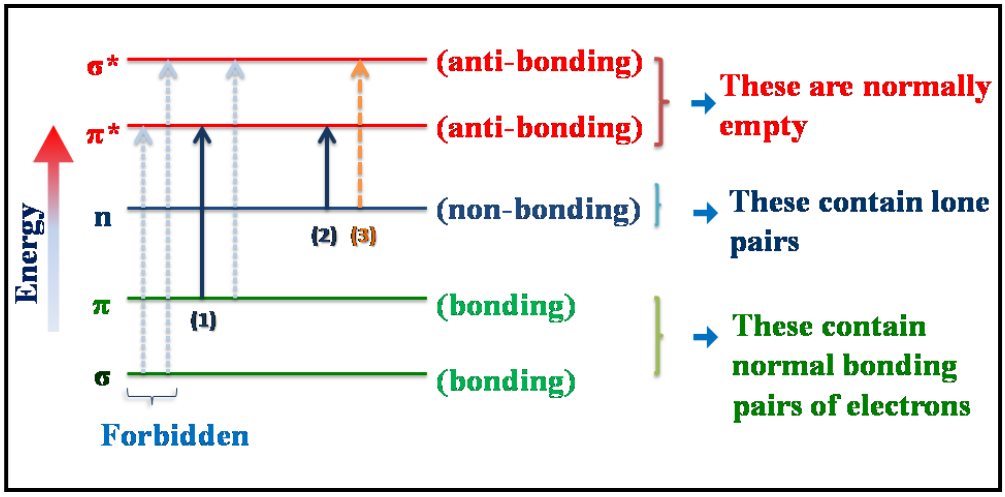

Figure 5.6 The hypothetical energy diagram of electronic transition.

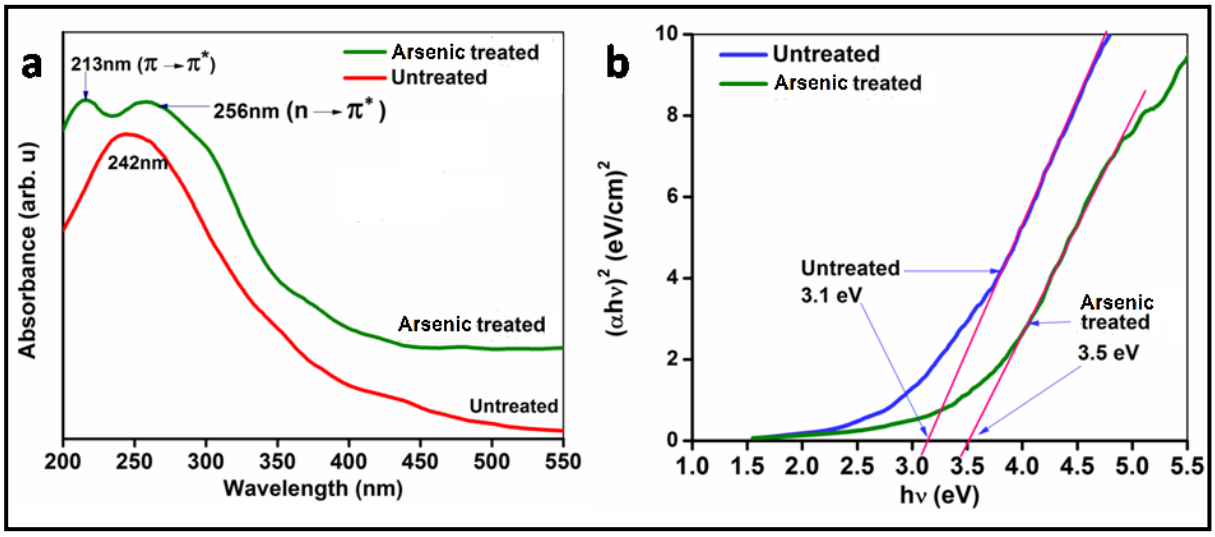

Figure 5.7 (a) UV-vis absorption spectra of untreated and arsenic treated frustules and (b) Tauc plot to determine the optical BG (direct) of untreated and arsenic treated diatom frustules respectively.

5.5.1 Calculation of optical bandgap using UV-visible spectra

The optical band gap was obtained from the absorption curve using Tauc relation given in equation 3.5 in chapter 3[14]. It was observed that the optical band gap increased to 3.5eV for arsenic treated diatom frustules from 3.1eV for untreated one (figure 5.7(b)). From UV-Visible analysis, it was found that the untreated diatom frustules had some similarities with properties of porous silica. SEM-EDS and XRD study confirmed that major parts of diatom frustules were composed of nano-sized pores of amorphous silica. In QC, when the size of the particle is comparable to the wavelength of electron wave function, material properties change from its bulk state. When a semiconductor or insulator is irradiated with photons, it leads to the formation of excitons by generating potential well and breaking the balance of inter-atomic Coulombic forces. Bound pair of electron and hole, called free excitons (FE), is initially delocalized and randomly fluctuates. When they come close to any distortions in the atomic positions having high distortion energy, they get self-trapped, which is the more stable state that reduces the excitonic energy [15, 16]. STE (self-trapped exciton) is the stabilization of excitons by localizing themselves in the potential well, due to the self-induced lattice distortion. Continuing this process, more excitons get localized and this leads to larger distortion until they are fully localized at the atomic scale and the system is locally distorted (i.e., broken bonds or formation of localized defects). This localized effect can be explained by formation of oxygen-related defects at the diatom frustule surface [15]. The Si-O bond is broken during the relaxation process. Moreover, trapping reduces excitation energy. This distortion effect lowers the BG of the porous silica structure in diatom frustules more than that of bulk silica structure. Also in case of arsenic treated diatom frustules absorption occurs due to the presence of arsenic which increases the BG from that of the raw diatom frustules.

5.6 Conclusions

Interesting properties of diatom frustules were found when incorporated with arsenic compound. Distinct changes were observed in arsenic treated diatom frustules when compared to untreated frustules. EDS analysis confirmed the presence of arsenic in the diatom frustules with 95% silica and 0.33% arsenic. Also change in optical BG from 3.1eV for untreated to 3.5eV for arsenic treated diatom frustules were observed. All these analyses show distinct and different characteristics of diatom frustules when they are treated with arsenic compounds. It can be concluded that diatoms can be used to detect arsenic in water bodies.

References

[1] Lowe, R.L. and Sherwood, A.R. Three new species of *Cosmioneis* (Bacillariophyceae) from Hawai'i. *Proceedings of the Academy of Natural Sciences of Philadelphia*, 160(1):21- 28, 2010.

[2] Mazumder, N., Gogoi, A., Buragohain, A. K., Ahmed, G. A. and Choudhury, A. Structural and optical characterization of fresh water diatoms (Cyclotella sp.): nature's nanoporous silica manufacturing plant. *Proc. Of SPIE*, 8996:89960Y-1, 2014. DOI:1117/12.2039793

[3] Bellamy, L. J. *The Infrared Spectra of Complex Molecules*, Chapman and Hall Ltd, London and New York, 2nd edition, 1980, ISBN-13:978-94-011-6522-8, DOl:1 0.1 007/978-94-011-6520-4

[4] Colthup, N., B., Daly, L., H. and Wiberley, S. E. *Introduction to Infrared and Raman Spectroscopy*. Academic Press, New York, San Francisco and London, 3rd edition, 1975.

[5] Gale, D. K., Gutu, T., Jiao, J., Chang, C. H. and Rorrer, G. L. Photoluminescence Detection of Biomolecules by Antibody-Functionalized Diatom Biosilica. *Adv. Funct. Mater*, 19:926- 933, 2009.

[6] Kumar, V., Kashyap, M., Gautam, S., Shukla, P., Joshi, K. B. and Vinayak, V. Fast Fourier infrared spectroscopy to characterize the biochemical composition in diatoms. *J Biosci.*, 43(4):717-729, 2018. DOI:10.1007/s12038-018-9792-z.

[7] Stuart, B. H. *Infrared Spectroscopy: Fundamentals and Applications*. John Wiley &Sons, Ltd., Sydney, Australia, 2004.

[8] Gelabert, A., Pokrovsky, O. S., Schott, J., Boudou, A., Feurtet-Mazel, A., Mielczarski, J., Mielczarski, E., Mesmer-Dudons, N. and Spalla, O. Study of diatoms/aqueous solution interface. I.Acid base equilibria and spectroscopic observation of freshwater and marine species. *Geochim. Cosmochim. Ac*., 68: 4039- 4058, 2004.

[9] Xia, S. Preliminary Characterization, Antioxidant Properties and Production of Chrysolaminarin from Marine Diatom *Odontellaaurita*. *Mar. Drugs.*, 12: 4883-4897, 2014.

[10] Jianying, Z. J., Ding, T., Zhang, Z., Xu, L. and Zhang, C. Enhanced Adsorption of Trivalent Arsenicfrom Water by Functionalized Diatom Silica Shells. *PLoS ONE*., 10: e0123395, 2015.

[11] Behzad, K.,Yunus, W. M. M., Talib, Z. A., Zakaria, A. and Bahrami, A. Effect of Preparation Parameters on Physical, Thermal and Optical Properties of n-type Porous Silicon. *Int. J. Electrochem. Sci.*, 7:8266- 8275, 2012.

[12] Okazaki, R. The development of new chemistry on multiple-bond compounds with heavier main group elements. *Tcimail number*., 105: 1- 15, 2000.

[13] Yamanaka, S., Yano, R., Usami, H., Hayashida, N., Ohguchi, M., Takeda, H. and Yoshino, K. Optical properties of diatom silica frustule with special reference to blue light. *J. Appl. Phys*., 103, 074701-5, 2008. DOI: 10.1063/1.2903342

[14] Borah, M. and Mohanta, D. Structural and optoelectronic properties of E^{u2+}- doped nanoscale barium titanates of pseudo-cubic form. *J. Appl. Phys*., 112: 124321- 8, 2012.

[15] Ismail-Beigi, S. and Louie, S.G. Self-Trapped Excitons in Silicon Dioxide: Mechanism and Properties. *Phys. Rev. Lett.*, 95: 156401- 4, 2005.

[16] Goswami, B., Choudhury, A. and Buragohain, A K. Luminescence properties of a nanoporousfreshwater diatom. *Luminescence*., 27:16- 19, 2012.